Next Materials 10 (2026) 101546

Contents lists available at ScienceDirect

Next Materials

journal homepage: www.sciencedirect.com/journal/next-materials

Research article

Electrospun polycaprolactone membranes as controlled delivery systems of polymyxin B for wound dressings applications

Julien G. Mahy [a,*], Stéphanie D. Lambert [a], Axel Lambert [b], Julie Bernard [a,b], Guérin Duysens [b], Ana Monteiro [b], Stéphane Dutrieux [b], Antoine Farcy [a], Raphaël Riva [c], Christine Jérôme [c], Olivier Jolois [b], Rémi G. Tilkin [b,*]

[a] Department of Chemical Engineering – Nanomaterials, Catalysis & Electrochemistry (NCE), University of Liège, Liège, Belgium
[b] Centexbel, Rue du Travail 5, Grâce-Hollogne 4460, Belgium
[c] Center for Education and Research on Macromolecules (CERM), University of Liège, Cesam-RU, Liège 4000, Belgium

ARTICLE INFO

Keywords:
Wound healing
Antimicrobial properties
Controlled release
Electrospinning

ABSTRACT

Electrospun polycaprolactone (PCL) nanofibrous membranes loaded with 2 2 % w/w polymyxin B (PMB) were developed as biodegradable antimicrobial wound dressings using two different solvent systems: organic (dichloromethane/dimethylformamide, OS) and acidic (acetic acid/formic acid, Acid). The choice of solvent significantly influenced fiber morphology, polymer crystallinity, mechanical properties, and drug-release kinetics. Both membranes exhibited well-defined bead-free nanofibers with diameters in the sub-micron range and porosity > 85 %. PMB release showed a marked initial burst within the first hour (≈ 35–55 % for OS membranes vs. ≈ 20–30 % for Acid membranes), followed by sustained diffusion over 7 days. Agar diffusion tests revealed strong antibacterial activity against Staphylococcus aureus (inhibition zone 1.5 mm for OS-PMB, growth inhibition under the sample for Acid-PMB) and Pseudomonas aeruginosa (5.0 mm and 0.6 mm, respectively), with no bacterial growth under any PMB-loaded samples. All membranes proved non-cytotoxic (> 80 % cell viability). The use of only two FDA-approved components, combined with a simple one-step electrospinning process and tunable release via solvent selection, offers a highly scalable and clinically translatable platform for the local delivery of polymyxin B in infected or at-risk wounds.

1. Introduction

The skin is the largest organ of the human body and acts as a barrier against external, aggressive agents [1]. When compromised, it loses its protective function, exposing the body to infection and inflammation [2]. The wound healing process is complex and highly sensitive to microbial contamination, especially from fungi (*Candida spp.*), Gram-positive (*S. aureus*), and Gram-negative (*P. aeruginosa*) bacteria [3–5]. These infections delay healing, increase morbidity, and may even lead to mortality [6].

Antibiotics—either systemic or topical—are traditionally used to combat wound infections. However, systemic antibiotics present the risk of promoting drug resistance due to overuse [3,7]. To address this, local drug delivery via wound dressings has emerged as a preferred alternative, offering targeted action and reduced systemic exposure [4].

Wound dressings serve multiple purposes: protection, moisture retention, gas exchange, and increasingly, antimicrobial action [6, 8–10]. A moist environment accelerates granulation and epithelialization [6]. Ideally, a dressing should be biodegradable, non-toxic, non-adherent to the wound, and easily replaceable [6,8,11].

Among dressing types—traditional, biological, and synthetic—synthetic membranes, especially nanofiber-based systems, offer promising features: small pore size to prevent microbial penetration, high porosity to promote gas exchange, and a structure resembling the extracellular matrix (ECM), favoring cell adhesion and proliferation [7–9].

Electrospinning is a versatile, cost-effective method to fabricate nanofibrous membranes with high surface area, tunable porosity, and controllable fiber morphology [12–15]. These scaffolds closely mimic the structure of the natural extracellular matrix (ECM), thereby promoting cell adhesion, proliferation, and differentiation—features particularly advantageous for skin tissue engineering and wound

* Corresponding authors.
E-mail addresses: julien.mahy@uliege.be (J.G. Mahy), rt@centexbel.be (R.G. Tilkin).

https://doi.org/10.1016/j.nxmate.2025.101546
Received 4 September 2025; Received in revised form 8 December 2025; Accepted 12 December 2025
Available online 19 December 2025

healing applications. Recent works have demonstrated its value in wound healing applications, including antibacterial membranes [16], multifunctional dressings [17,18], and composite scaffolds designed to mimic the native skin environment [19,20].

However, electrospun biomaterials also present limitations, such as insufficient mechanical strength, limited control over pore size for cell infiltration, and challenges related to large-scale production or reproducibility. To address these, recent works have explored functionalization strategies or co-electrospinning of multiple polymers to improve mechanical and biological performance. For example, Pan et al. [21] developed a core–shell nanofiber system for dual drug release, enhancing antibacterial and angiogenic properties. Li et al. [22] reported electrospun mats incorporating bioactive peptides for enhanced skin regeneration. Rahman et al. [23] demonstrated a multifunctional scaffold with improved hemostatic and antimicrobial properties.

These studies illustrate the current trend toward multifunctional electrospun scaffolds, though they often rely on complex architectures or costly bioactive additives. In contrast, our work presents a simplified, yet efficient antimicrobial dressing using only FDA-approved materials and a two-component formulation, polycaprolactone (PCL) and polymyxin B (PMB), aiming to balance efficacy with scalability and biocompatibility.

PCL is a synthetic, aliphatic polyester widely used in biomedical applications due to its biocompatibility, biodegradability, and mechanical robustness [24,25]. Compared to natural polymers such as gelatin or collagen, PCL offers several advantages: higher stability in aqueous environments, tunable degradation rate (weeks to months), and mechanical properties that can be adjusted to match soft tissue elasticity [24]. Moreover, it does not require crosslinking agents to maintain structural integrity in humid or physiological conditions, unlike gelatin or collagen, which often degrade too quickly or require chemical modification to be stable [24,25]. However, one limitation of PCL is its hydrophobic nature, which can hinder cell adhesion—but this is often counterbalanced by the high surface area and porosity of electrospun scaffolds.

As for the antimicrobial agent, PMB is a cationic lipopeptide with high affinity for the lipopolysaccharide layer of Gram-negative bacteria [26,27]. Unlike silver ions or iodine, PMB is a biological molecule with a well-characterized pharmacological profile and low cytotoxicity at therapeutic concentrations. Compared to broad-spectrum antibiotics like gentamicin or sulfadiazine, PMB offers a selective action against multi-drug resistant Gram-negative bacteria, including *P. aeruginosa*, a common and problematic pathogen in burn wounds [26,27]. Importantly, PMB can be incorporated directly into the polymer matrix without complex encapsulation or chemical modification.

The design of our dressing relies on three core principles: (i) using a minimal formulation composed only of PCL and PMB, (ii) leveraging electrospinning to produce highly porous, nanofibrous membranes with high drug-loading efficiency, and (iii) modulating polymer degradation and drug release profiles through the choice of solvent system. Unlike other strategies involving nanoparticles, drug carriers, or surface grafting, our approach is simple, reproducible, and scalable, and uses FDA-approved materials only, which facilitates potential clinical translation.

While various electrospun dressings have been reported, many rely on complex encapsulation strategies (e.g., nanoparticles, clays) or incorporate agents with environmental or cytotoxic drawbacks [28,29]. Moreover, the impact of solvent systems on polymer degradation, fiber morphology, and drug release is often neglected, despite being critical for therapeutic efficacy [30–32].

In this work, we aim to develop electrospun membranes based on polycaprolactone (PCL) and loaded with polymyxin B (PMB), a potent antimicrobial peptide. The membranes are produced using two solvent systems – organic (dichloromethane / dimethylformamide) and acidic (acetic acid / formic acid) – to investigate how solvent choice affects polymer degradation, fiber morphology, drug release, and antimicrobial performance. This organic solvent system has been chosen has it is widely used in the literature [33–35]. Yet, this system is known to be toxic. The acidic system has therefore been chosen in order to reduce the toxicity of the process. The principle of production and action is illustrated in Fig. 1.

Our objectives are to: (i) Compare the effects of solvent systems on PCL degradation during electrospinning, (ii) Characterize the morphology, porosity, and mechanical properties of the membranes, (iii) Evaluate the kinetics of PMB release and its antimicrobial efficiency against S. aureus and P. aeruginosa, (iv) Assess the cytotoxicity of the membranes to ensure biocompatibility.

Compared to existing approaches, our system stands out for its simplicity, full biodegradability, and use of FDA-approved materials, without requiring complex carriers or post-treatments. This offers a practical, scalable route toward safe and efficient antimicrobial wound dressings.

2. Materials and methods

2.1. Materials

Polycaprolactone (PCL, $(C_6H_{10}O_2)_n$ Mn = 80 kDa) were purchased from Sigma-Aldrich; Polymyxin B sulphate (PMB, $C_{56}H_{100}N_{16}O_{17}S$) from Apollo Scientific; dimethylformamide (DMF, $HCO\text{-}N(CH_3)_2$), dichloromethane (DCM, CH_2Cl_2), acetic acid glacial (AA, CH_3COOH) from VWR; formic acid (FA, HCOOH, ≥ 98 %) from Carl Roth; tetrahydrofuran (THF, C_4H_8O) and Triton X-100 ($C_{14}H_{22}O(C_2H_4O)_n(n = 9–10)$) from Fischer Scientific; Dulbecco's Modified Eagle medium (DMEM) and Fetal Bovine Serum (FBS) from Biowest; Penicillin/Streptomycin and amphotericine from Capricorn; XTT assay from Roche; S. aureus (ATCC 25923) and (P. aeruginosa) (ATCC 25922) from ATCC. Unless indicated otherwise, all these chemicals were ≥ 99 % pure and were used without further purification.

Phosphate Buffer Saline (PBS) was prepared from PBS tablets purchased from PanReac AppliChem.

2.2. Methods

2.2.1. Electrospinning process

The electrospinning unit (Fig. 2) is a homemade vertical set-up composed of a collector (aluminum plate with adjustable height) and a needle (21 G) fed with the polymer solution at a constant flow rate thanks to a push-syringe (NE-1800 from Quality In Sensing). The collector is connected to a high voltage supply (SL80PN60 from Spellman) while the needle is connected to the ground. The needle is mounted on a XY motor for the production of large membranes. The needle was moved along the X axis over a length of 20 cm at a speed of 10 cm/min. The electrospinning unit is housed in a hermetically sealed enclosure where temperature and humidity levels are controlled by a regulating system.

Two solvent systems were used in this work: 50/50 AA/FA (called Acid) and 50/50 DMF/DCM (called OS). All solutions were composed of 17 % m/v of PCL. In the case of the PMB containing samples, 0.34 % m/v of PMB were added in the solution, which corresponds to a ratio m_PMB/m_PCL of 2 %. The PMB concentration was selected to ensure effective performances while minimizing disruption to the electrospinning process. Several studies showed a decrease in the viscosity of the solution over time due to the acidic hydrolysis of PCL [30,31]. To guarantee the reproducibility of the results, the duration of the mixing step was fixed at 16 h and kept constant for all samples and all replicates. The possible degradation of PCL was evaluated (see next section).

The flow rate was set to 0.014 mL/min for the Acid system and to 0.016 mL/min for the OS system. The distance between the needle and the collector was fixed at 14.5 cm for the Acid system and 16 cm for the OS system. The temperature was set to 25 °C and the relative humidity to 20 %. The duration of electrospinning was 3 h. The specific solution composition and voltage for each membrane are shown in Table 1. The choice of these parameters is based on a preliminary optimization,

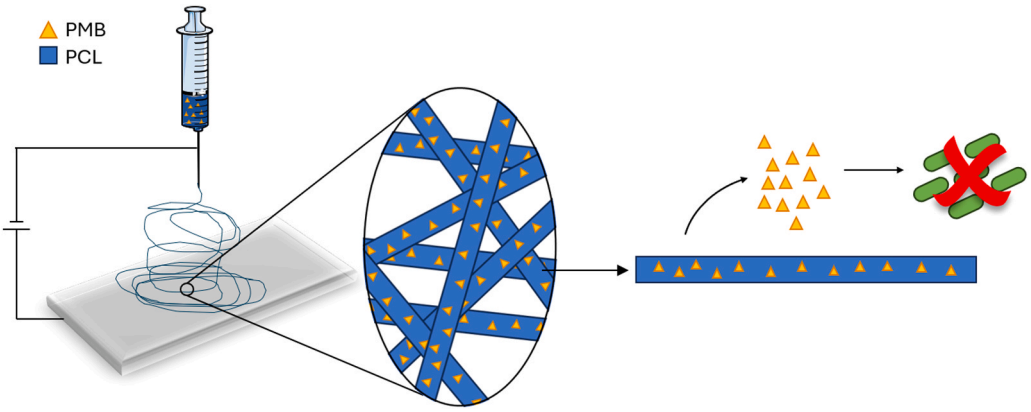

Fig. 1. General principle of the studied process.

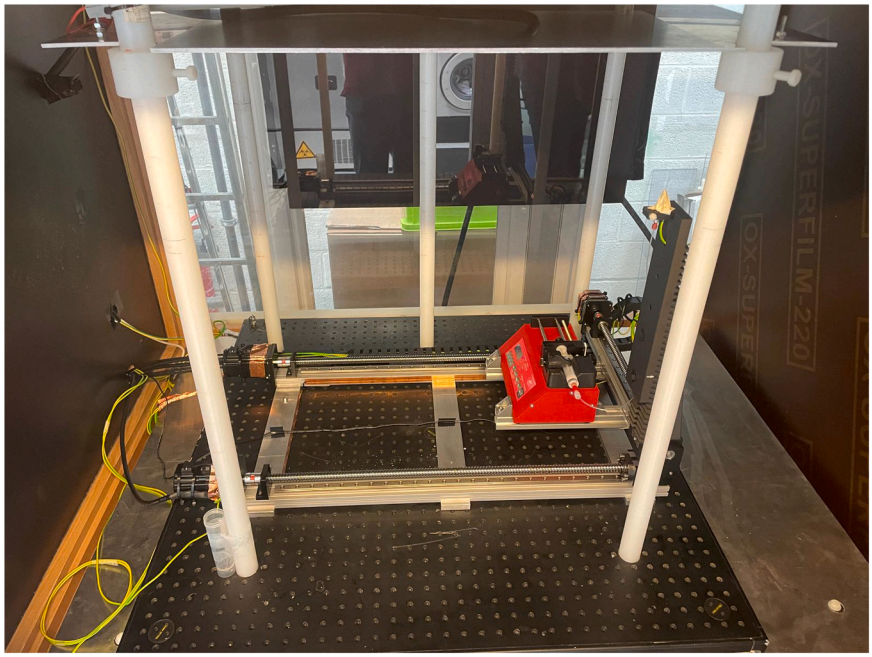

Fig. 2. Electrospinning experimental set-up.

Table 1
Solution composition and voltages.

Sample	Solvent system	% m/v PMB	V (kV)	Flow rate (mL/min)
Acid	50/50 AA/FA	0	16	0.014
Acid-PMB	50/50 AA/FA	0.34	16	0.014
OS	50/50 DMF/DCM	0	12	0.016
OS-PMB	50/50 DMF/DCM	0.34	11	0.016

shown in 1 in the supplementary information.

2.2.2. Physico-chemical characterization

The viscosity of the polymer solutions was measured at 10 rpm under room temperature using a RVDV2T viscosimeter from Brookfield and a C spindle.

The fiber morphology was investigated via scanning electron microscopy (SEM, TESCAN Clara microscope) with accelerating voltage of 15 kV, after being sputter coated for 1 min with gold using an AGAR high-resolution sputter-coater. The fiber diameters were measured on SEM images using Image J image analysis software. For each sample, a total of 100 measurements were made on 4 different SEM images, each representing a non-overlapping random field of view for each electrospun membrane configuration.

The porosity (percentage of void) was determined by recording the mass of the membrane before and after immersion in ethanol for 15 min. The following equation was then used to calculate the porosity via Eq. 1.

$$Porosity(\%) = \frac{(m_{EtOH} - m_{dry})/\rho_{EtOH}}{(m_{EtOH} - m_{dry})/\rho_{EtOH} + m_{dry}/\rho_{mem}} \times 100 \quad (1)$$

where m_{dry} is the mass of the dry membrane (g), m_{EtOH} is the mass of the membrane after immersion in ethanol (g), ρ_{mem} is the density of PCL (i.e. 1.145 g/cm^3) and ρ_{EtOH} is the density of ethanol (i.e. 0.789 g/cm^3). This measurement was carried out on 3 samples.

Membrane thicknesses were measured using a digital micrometer (MDC-25PX from Mitutoyo) with the membranes placed between two microscope slides. The thickness of the two microscope slides was subtracted to the measurement value. This measurement was carried out on 3 samples.

2.2.3. Mechanical properties and conformability

The mechanical properties of the membranes in traction mode were measured using a 3366 model from Instron, equipped with a load cell which had a maximum load of 100 N and a repeatability of 0.25 %. The test speed was 100 mm/min and the gripping distance was 20 mm. The tested samples were rectangular-shaped specimens measuring 7 cm in length and 2 cm in width. The representative stress–strain curves were reported for each sample. This measurement was carried out on 3 samples.

The conformability was studied by determining the extensibility and permanent set, based on the norm ISO 13726:2023 using a 3366 model from Instron, equipped with a load cell which had a maximum load of 100 N and a repeatability of 0.25 %. Shortly, 2 parallel marks were drawn on the sample. The distance between the two marks (L_i) was measured. The sample was then extended by 20 % of the marked distance at a rate of 300 mm/min and the maximum load was measured. The sample was then held at this extension. After 60 s, the sample was removed and let to relax for 300 s. The distance between the two marks was measured again (L_f). The extensibility was given by Eq. 2.

$$\text{Extensibility (N/cm)} = \text{maximum load / sample width} \quad (2)$$

The permanent set was given by Eq. 3.

$$\text{Permanent set (\%)} = (L_f\text{-}L_i)/L_i \text{ x } 100 \quad (3)$$

This measurement was carried out on 4 samples.

2.2.4. Degradation study

The degradation of the PCL during the electrospinning process was checked by differential scanning calorimetry (DSC), thermogravimetric analysis (TGA), and gel permeation chromatography (GPC). DSC was realized using a Discovery DSC2500 from TA instruments, following the norm ISO 11357–1:2023. The rate of heating was 10 °C/min from −90–100 °C, where a typical sample weight was around 2 mg. Peak height and peak area in the thermogram were ascribed to the melting point (T_m) and melting enthalpy (ΔH_m), respectively. The degree of crystallinity X_C was calculated via Eq. 4.

$$X_C\ (\%) = \Delta H_m \,/\, \Delta H_m^0 \text{ x } 100 \quad (4)$$

with ΔH_m the measured melting enthalpy and ΔH_m^0 the melting enthalpy of fully crystalline PCL (139.5 J/g) [36].

TGA was performed using a TGA5500 from TA instruments with a heating rate of 10 °C/min under nitrogen atmosphere between 30 and 600 °C and under air atmosphere between 600 and 900 °C.

SEC was carried out in THF at 45 °C at a flow rate of 1 mL/min with a Viscotek 305 TDA liquid chromatograph equipped with 2 PSS SDV linear M columns calibrated with polystyrene standards. Samples were dissolved in THF, filtered with a 0.22 μm filter.

The presence of specific functional groups was checked by Fourier transformed infrared (FTIR) spectroscopy in ATR mode (iD7 ATR from ThermoScientific) using a Nicolet iS5 from ThermoScientific. The following instrumental settings were used: absorbance, range from 4000 to 400 cm^{-1}, 16 scans, resolution 2 cm^{-1}. The spectra were normalized to the peak corresponding to C═O stretching (around 1720 cm^{-1}).

2.2.5. Release

The kinetics of PMB release were determined by immersing 0.1 g of sample in 10 mL of PBS solution in closed vials. This analysis was performed in duplicates. Membranes were incubated at 37 °C. At scheduled times (i.e. 30 min, 1 h, 4 h, 24 h, 2 days, 3 days, 7 days), the supernatant was removed, stored at −20 °C until analysis, and replaced by fresh PBS. The antimicrobial concentration was assessed via the Lowry method (absorbance measurement at 750 nm, UV-1800 from Shimadzu; Modified Lowry Protein Assay Kit from Thermo Scientific) [37]. A second order calibration curve ($R^2 = 0.9999$) was produced by using PMB as standard (1, 2, 5, 10, 25, 50, 100, 150, 200, 250 μg/mL).

2.2.6. Antimicrobial activity

Prior to antimicrobial testing, all samples were sterilized by UV irradiation for 20 min (10 min on each face). Specimen were cut into a disk 25 mm in diameter.

Antimicrobial activity of the sample was assessed by agar diffusion plate test, following the norm ISO 20645:2004. The level of antibacterial activity was assessed by examining the extent of bacterial growth in the contact zone between the agar and the specimen, and if present, the extent of the inhibition zone around the specimen. Two bacterial strains were used for the assay: *Staphylococcus aureus* (ATCC 6538) and *Pseudomonas aeruginosa* (ATCC 9027). Bacteria were grown overnight in tryptone soy agar (TSA) at 37 °C. Then, one colony was used for inoculation of a trypticase soy broth (TSB) incubated at 37 °C to reach sufficient turbidity. TSA agar plates were inoculated with bacterial suspension. Samples were laid down on inoculated plates. Plates were incubated at 37 °C. After 24 h and 48 h, plates were analyzed under binocular magnifier and the inhibition zone around the specimen was measured. Measurements were carried out on 3 references.

2.2.7. Cytotoxicity

Prior to cytotoxicity testing, all samples were prepared following the norm ISO 10993–12:2021. Sterilization by UV irradiation for 30 min was carried out before extraction.

The cytotoxicity was assessed via the enumeration of remaining living cell after contact with an extract of the sample, following the norm ISO 10993–5:2009. First, an extract of the membrane was prepared by placing 1.25 cm^2/mL of material in full growth culture medium (DMEM, 10 % FCS, penicillin, and streptomycin) at 37 °C – 200 rpm for 24 h.

The cytotoxicity was then measured by the cell viability by dehydrogenase mitochondrial activity of fibroblast cells (L929 clone) using XTT assay. Cells were seeded in 12-well tissue culture plates at a concentration of 1×10^5 per well and incubated overnight in full growth medium at 37 °C, 5 % CO_2. Medium was removed and extracts were added to the cells for 24 h (37 °C, 5 % CO_2). Positive control (HDPE film), negative control (Triton X-100 0.05 %), and non-treated controls (culture medium) were conducted simultaneously. All samples were carried out in triplicates. After 24 h of treatment, 50 μl of XTT solution was added in each well and plates were incubated in darkness for 2 h (37 °C). Reading absorbance of the plates was conducted by using plate spectrophotometer at 450 nm. The absorbance of cells in contact with culture medium alone was used as blank.

A decrease in the number of living cells causes a decrease in total dehydrogenase activity mitochondria of the sample. This reduction is directly linked to the quantity of XTT byproduct formed, which is measured by optical density at 450 nm (Spectrophotometer Spectramax 340PC 384 from Molecular Devices). To calculate the reduction in viability compared to the blank, Eq. 5 was used:

$$\text{Viability (\%)} = \text{OD450e / OD450b x } 100 \quad (5)$$

Where OD450e is the mean optical density of the extract, OD450b is the mean optical density of the blank. The lower the viability percentage is, the higher the cytotoxic potential of the sample under test is. The norm ISO 10993–5 states that if the viability is < 70 %, the sample has cytotoxic potential.

2.2.8. Statistical significance

To assess the statistical significance, a one-way analysis of variance (ANOVA) followed by post hoc Tukey's test was conducted, using a significance level of $p = 0.05$. The assumption of homogeneity of variances was tested beforehand using Levene's test.

3. Results and discussions

3.1. Degradation of PCL

The degradation of PCL during the electrospinning process was investigated through DSC, TGA, and SEC measurements. The DSC and SEC results can be seen in Table 2. Regarding TGA, a typical TGA curve is presented in Fig. 3 while all the curves are presented in 2 of the supplementary information (Figure SI-1).

The resulting molar mass was greatly influenced by the solvent system chosen to perform electrospinning. Indeed, compared to the raw material (PCL pellet), a significant decrease of about 10 kDa was observed for the samples prepared in acidic conditions (Acid and Acid-PMB), while no significant degradation was detected for the one prepared with organic solvents (OS and OS-PMB). No significant degradation was found between the sample with or without PMB. This degradation is due to the ester hydrolysis of the PCL (primary degradation pathway) [38,39]. This reaction is catalyzed by acids (especially at pH < 3 like in this case) and is known to result in a decrease of the molar mass. As the OS and OS-PMB membranes do not present a degradation, it is hypothesized that the electrospinning process does not have an influence on the molar mass. To check this hypothesis, films were prepared in the same preparation conditions (PCL film Acid = film prepared in Acid conditions; PCL film OS = film prepared in OS conditions). Here again, a significant decrease was observed for the Acid conditions, while no significant degradation was detected for the OS conditions. The decrease was even larger for the films than for the electrospun membrane because PCL stayed longer in contact with the acids due to their slow evaporation rate. This shows that the degradation of PCL was indeed caused by the choice of medium rather than by the electrospinning process. Several studies showed similar results [30,31]. They also found a decrease in the viscosity of the solution over time due to this acidic hydrolysis. To guarantee the reproducibility of the results, the duration of the mixing step was kept constant for all samples and all replicates.

The effect of the choice of solvent on the calorimetric properties was also investigated by DSC. The thermal analysis showed a significant increase in crystallinity (X_c) between the raw PCL and the OS / OS-PMB membranes. No significant degradation was found between the sample with or without PMB. During the electrospinning process, the PCL molecular chains are stretched during the flight of the polymeric solution. The membranes once formed present more aligned chains than a randomly processed pellet, promoting the formation of crystalline areas [40,41]. A significant increase in crystallinity was also observed between the raw PCL and the Acid / Acid-PMB membranes. This increase was larger than the one of the OS / OS-PMB membranes. No significant degradation was found between the sample with or without PMB. In this case, besides the effect of the electrospinning process, the lower molar mass enhances chain packing and leads to the formation of more perfect lamellar crystal structures, which require higher temperatures to melt [32]. Despite these changes in crystallinity, no change in melting temperature (T_m) could be detected, indicating that the crystalline zones were similar (Table 2). The significantly higher crystallinity of the Acid / Acid-PMB compared to the OS / OS-PMB membranes can be explained by the volatility of the solvent. Indeed, the higher the volatility of the solvent, the faster it evaporates during fiber formation, resulting in fibers with lower crystallinity [40,42].

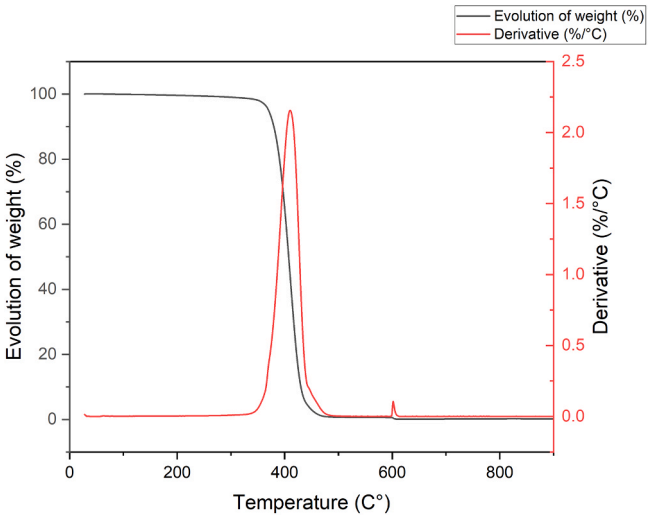

Fig. 3. Typical TGA curve (black line) and its derivative (red line). Sample = PCL pellet.

All these changes did not affect the TGA results (Fig. 3 and 2 of the supplementary information), showing that the thermal degradation of the membrane was not affected by the addition of PMB and the choice of solvent. For all the samples (typical curve in Fig. 3), a single degradation step in the range from 320 to 480–490 °C with a temperature of maximum decomposition rate of 409–411 °C was observed, which corresponds to previous studies [43–45]. It has been shown that this degradation is due to two simultaneous processes: (i) the statistical rupture of the polyester chains yielding H_2O, CO_2, hexenoic acid, and small chain fragments of PCL and (ii) the release of ε-caprolactone as results of an unzipping depolymerization process [43,44].

The presence of specific functional groups was checked by FTIR (see 3 in the supplementary information). The FT-IR peaks in the membrane spectra were similar to those in the spectrum of the pure PCL pellets, suggesting that there were no significant structural changes due to the choice of solvent or the addition of PMB in PCL matrix, such as new chemical bond formation between the PCL chains and PMB [46,47].

3.2. Morphology

The PCL membranes produced by electrospinning were analyzed using scanning electron microscopes to evaluate the quality and regularity of the fibers. The fiber diameter was measured using ImageJ software and denoted in Table 3. The images of the 4 samples are represented in Fig. 4.

Acid and Acid-PMB membranes (Figs. 4a and 4b) showed intertwined non orientated fibers, with some beads, as previously observed during the electrospinning of PCL in organic acids [30,48]. These beads form when surface tension forces are strong enough to displace the solution along the jet, creating localized regions with minimal surface-to-volume ratio [48]. The addition of PMB seemed to produce

Table 2
DSC and SEC results (mean ± standard deviation).

Sample	M_n (kDa)	T_m (°C)	X_c (%)
PCL Pellet = raw material	73.8 ± 2.3	56.3 ± 0.1	51.5 ± 0.5
Acid	62.6 ± 3.8	57.0 ± 0.1	58.5 ± 0.4
Acid-PMB	63.8 ± 2.1	57.4 ± 0.2	59.8 ± 0.6
OS	71.8 ± 3.4	58.1 ± 0.1	55.7 ± 0.5
OS-PMB	81.7 ± 7.1	57.4 ± 0.1	56.6 ± 0.7
PCL film Acid	52.7 ± 1.8	/	/
PCL film OS	74.5 ± 1.1	/	/

Table 3
Morphology data (mean ± standard deviation).

Sample	Fiber diameter (μm)	Porosity (%)	Membrane thickness (μm)	Viscosity (Pa.s)
Acid	0.218 ± 0.055	92 ± 1	50 ± 7	1.284
Acid-PMB	0.188 ± 0.025	93 ± 1	80 ± 7	1.206
OS	1.490 ± 0.289	91 ± 1	120 ± 8	2.605
OS-PMB	1.226 ± 0.579	91 ± 2	150 ± 10	1.833

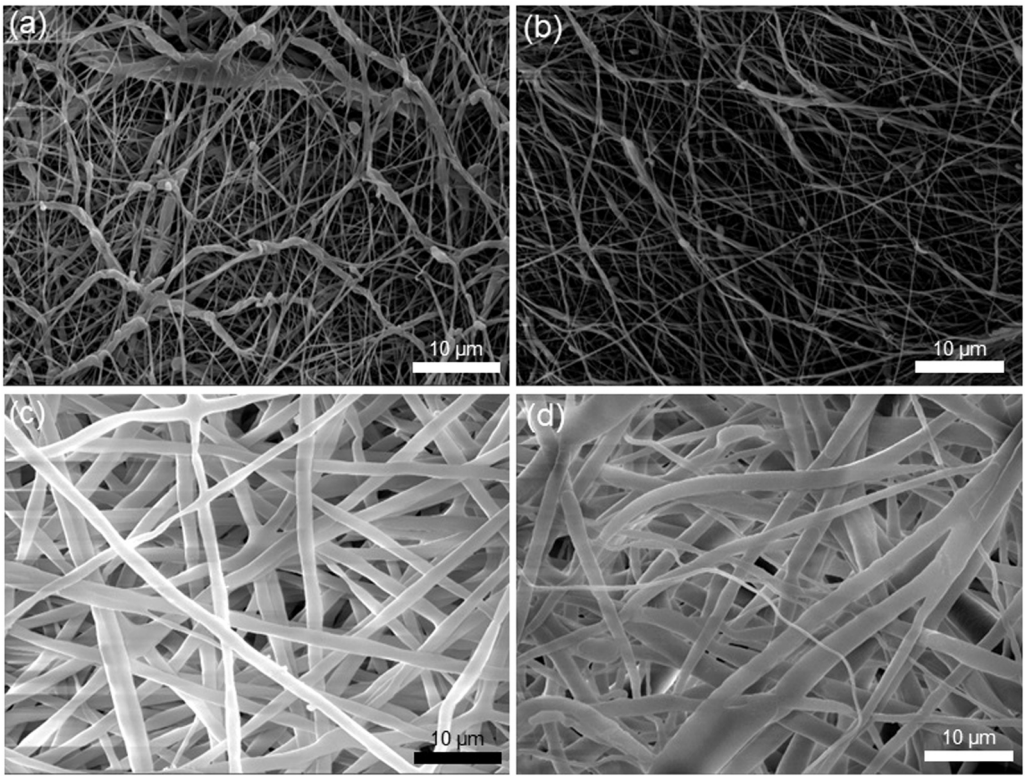

Fig. 4. SEM images of (a) Acid, (b) Acid-PMB, (c) OS, and (d) OS-PMB samples.

slightly less regular fibers. The presence of beads on the Acid and Acid-PMB membranes could affect the release of antimicrobials and, therefore, adjustments in the electrospinning process could be considered to obtain membranes composed of uniform fibers without beads. Regarding the fiber size, these samples presented an uneven fiber size distribution, where some densely intertwined areas make diameter measurement difficult. However, less dense areas revealed an average diameter of 0.218 ± 0.055 µm (Acid) and 0.188 ± 0.025 µm (Acid-PMB), without significant difference, showing that the addition of 2 % of PMB did not impact the morphology. These values are consistent with previous studies using organic acids [30,48,49].

For the membranes from solvent solutions (OS and OS-PMB), a clear difference was observed in the morphology of the fibers compared to those from acidic solutions (Figs. 4c and 4d), especially regarding the fiber size as the average diameter was 1.490 ± 0.289 µm (OS) and 1.226 ± 0.579 µm (OS-PMB). These diameters were significantly larger than the ones observed for the membranes from acidic solution. Yet, no significant difference was observed between OS and OS-PMB, showing that the addition of 2 % of PMB did not impact the morphology. These values are consistent with previous studies using organic solvents [46, 49,50].

The difference of morphology between the membranes produced with Acid and OS solutions can be explained by several factors. First, this difference comes from the fact that acidic solutions display lower viscosities than those containing solvents (Table 3), which promotes the formation of finer fibers with pearls. It has been proven that increased molecular entanglement suppresses the early development of bending instability, extending the stable jet region and leading to the formation of thicker fibers [30,51]. The lower viscosity of the Acid membranes compared to the OS membranes can be linked to the decrease of molar mass, as previously presented in the degradation study. Another parameter aligned with this behavior is electrical conductivity. Indeed, it has been shown that the average fiber diameter increases as conductivity decreases, as it can be hypothesized for the DCM/DMF solution compared to the AA/FA based on their dielectric constant [50,51]. Finally, the larger flow rate for the OS/OS-PMB membranes compared to the Acid/Acid-PMB ones also promotes larger fibers as, an increased flow rate delivered a larger volume of polymeric solution to the jet, which in turn results in thicker fibers, as was previously observed [52, 53].

The porosity of the membrane was also measured using a liquid impregnation technique. Knowing the porosity of the membranes is essential to understand their permeability. The void fractions are presented in Table 3. The results showed a high void fraction for all the membranes (i.e. 91–93 %), similar to values obtained in previous studies [46,54,55]. No significant difference between the samples could be observed, showing that the electrospinning parameters have little impact on the porosity.

The thickness of PCL membranes determined using a micrometer is summarized in Table 3. As a reminder, the membranes were all electrospun for an equal duration. The membranes produced from organic solvents were significantly thicker than the ones produced from acids. This can be explained by the geometric constraints caused by the thicker fibers of the OS/OS-PMB membranes, resulting in increased thickness. Another explanation comes from the lower width of the produced membranes (around 6 cm for OS/OS-PMB membranes and 9 cm for the Acid/Acid-PMB membranes), leading to a larger accumulation of matter on a smaller surface area and therefore to a thicker membrane. Comparing the thickness of electrospun membranes with other studies is quite hard given the fact that it depends on the duration of electrospinning and the surface on which the electrospinning is performed, which are hardly provided.

3.3. *Mechanical properties and conformability*

The typical strain-stress curves are shown in Fig. 5 and the mechanical properties and the conformability in Table 4.

The stress–strain response of the fibrous scaffolds exhibited two distinct stages: an initial linear elastic region followed by a nonlinear plastic deformation phase, typically ending with the fracture of the

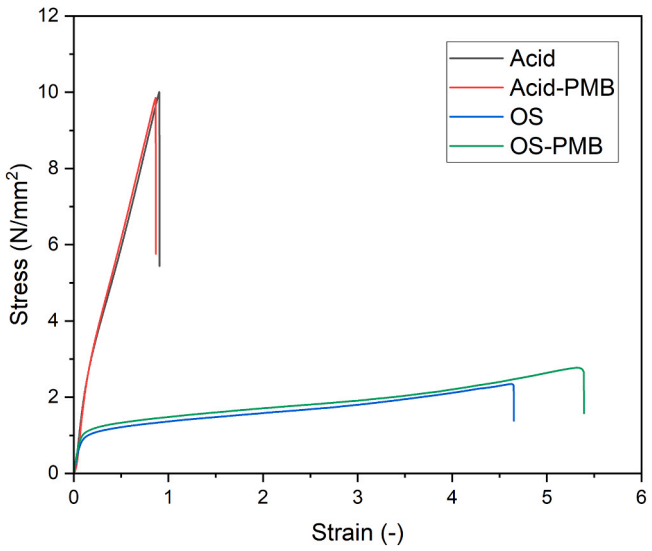

Fig. 5. Typical stress-strain curves. (black) Acid, (red) Acid-PMB, (blue) OS, and (green) OS-PMB.

Table 4
Mechanical properties and conformability of the membranes (mean ± standard deviation).

Sample	Young's Modulus (MPa)	Strain at break (%)	Stress at break (MPa)	Extensibility (N/cm)	Permanent set (%)
Acid	21.1 ± 3.7	83.9 ± 11.9	9.1 ± 2.7	3.4 ± 0.3	3.7 ± 0.7
Acid-PMB	20.9 ± 3.8	85.1 ± 11.1	8.0 ± 1.7	3.4 ± 0.2	3.7 ± 0.4
OS	11.8 ± 0.7	406.7 ± 50.7	2.2 ± 0.2	2.1 ± 0.1	2.9 ± 0.5
OS-PMB	12.0 ± 1.5	462.0 ± 67.3	2.3 ± 0.3	2.0 ± 0.3	1.7 ± 0.8

membrane.

When comparing the membrane types, a significant difference between the Acid / Acid-PMB and the OS / OS-PMB membranes could be noticed. The Acid and Acid-PMB membranes indeed showed a significantly larger Young's modulus, a significantly larger stress at break, and a significantly lower strain at break, indicating that they were stiffer and more brittle. It can be hypothesized that this observation is due to the fact that the Acid membranes are composed of more crystalline fibers than the OS and OS-PMB membranes (see Table 2) [47]. It has also been shown that a higher voltage, as it is the case for the Acid/Acid-PMB membranes compared to the OS/OS-PMB ones is linked to higher mechanical properties [46,56,57]. Indeed, at high voltages, conglutination frequently arises during the electrospinning of scaffolds, enhancing the material's tensile strength and Young modulus through the development of a network of interwoven fibers.

Regarding the addition of PMB, no significant difference could be observed. This is linked to the fact that they present similar porosity, fiber diameters, and crystallinity.

Compared to commercially available wound dressings, all the membranes showed properties similar to the ones measured on commercial wound dressings (1–35 MPa for the Young's modulus, 1–8 for the strain at break, 0.1–5 MPa for the stress at break) [58]. The higher stress at break for the Acid and Acid-PMB membrane does not pose a problem as it simply means that it will be more resistant. These values were also consistent with the properties of the skin present in the literature (3–50 MPa for the Young's modulus, 0.2–2 for the strain at break, 1–32 MPa for the stress at break) [59].

The conformability can be determined via two parameters: the extensibility and the permanent set. The extensibility is the force needed to deform a material to a given extension. The higher the value, the lower the extensibility. The permanent set is the increase in length of a material after it has been stretched and relaxed. A low value for permanent set indicates that the wound dressing can recover its original shape and properties after being stretched.

When comparing the membrane types, it could be observed that the Acid and Acid-PMB membranes presented a significantly higher extensibility than the OS and OS-PMB membranes. This could be explained by the fact that Acid and Acid-PMB membranes are less elastic than the OS and OS-PMB ones (higher Young's modulus). The difference between the Acid membrane and the OS membrane permanent set was not significant.

As for the mechanical properties, the addition of 2 % of PMB did not have a significant effect on the conformability.

Compared to commercially available wound dressings, all the membranes showed values in the range suitable for a flexible dressing. They were comparable to commercial foam (2.2–4.0 N/cm for extensibility and 1.5–3.9 % for permanent set) and hydrocolloid (0.9–3.7 N/cm for extensibility and 0.1–7.6 % for permanent set) wound dressings.

The mechanical properties and conformability of wound dressing are essential properties for wound dressings. First, these properties define its ability to be handled by nurses/doctors/patients [60–62]. The wound dressing must indeed have sufficient resistance to be correctly handled without a risk of breaking. These properties also influence the patient's comfort and mobility. When applied to a part of the body that moves, such as a joint, the dressing should allow sufficient freedom for movement. A dressing that stretches easily and returns to its original length after being stretched would be more comfortable for the patient to wear. The selection of where it should be placed therefore depends on these properties, as non-flexible wound dressing should rather be placed in fixed area.

These properties also define the dressing's ability to mold to the shape of the wound and the surrounding skin, creating a secure fit that ensures it stays in close contact with the tissue [62]. This is important to maintain moist conditions required for healing, prevent the formation of dead space where wound fluid and bacteria may accumulate (reducing the risk of infections), and avoid leakage of wound exudate (minimizing the risk of maceration).

3.4. PMB release

Fig. 6 illustrates the release kinetic profiles. To ensure clarity, these figures are divided in two parts: (a) profiles over the full period (7 days) and (b) amount of PMB released after the first hour. This second figure is expressed as the amount of PMB released after 1 h, with the amount of PMB released up to 1 h being subtracted.

Both release kinetics profiles highlighted a fast release of PMB within the first hour, called burst, followed by a slower release up to 7 days. It is assumed that this burst is mostly due to the fraction of the PMB present on or close to the external surface of the electrospun fibers, which can easily and rapidly desorb upon immersion. Based on the fiber size, it would be expected to observe a faster release from the Acid membrane because they present a smaller diameter and therefore a larger surface area. This phenomenon actually comes from the difference in solubility in the polymer matrix. Indeed, PMB is soluble in the Acid solution (AA and FA), the active agent is therefore uniformly dispersed in the PCL matrix. On the contrary, PMB is not soluble in the OS medium (DCM and DMF). The PMB is therefore dispersed in the PCL matrix under the form of small aggregates. It is expected that these aggregates are large enough to be at the surface of the fibers, leading to a large amount of released PMB at the beginning. This burst ensures a fast antimicrobial activity of the wound dressing.

When looking at the amount of PMB released after the first hour, it can be noticed that the release profiles of the Acid-PMB and OS-PMB

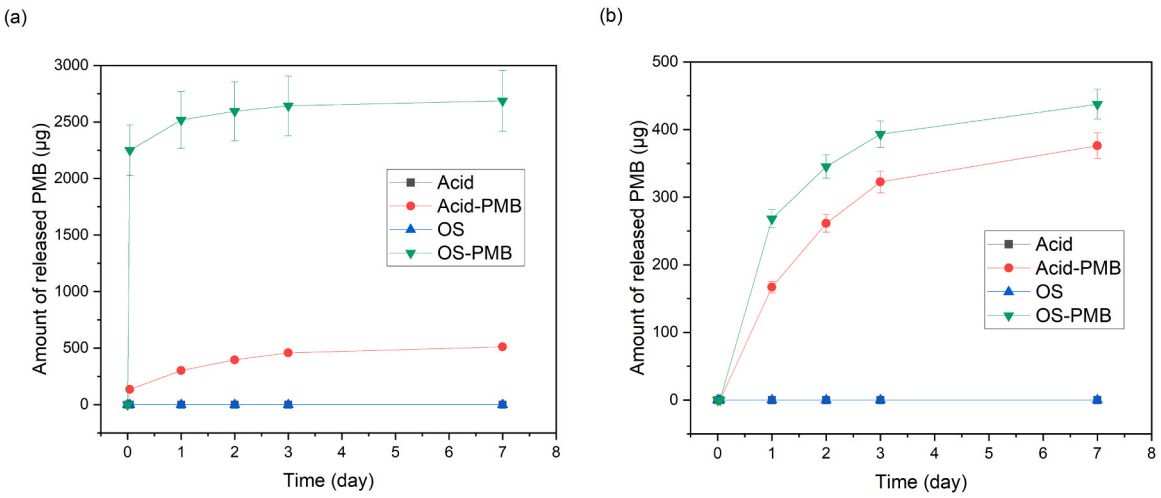

Fig. 6. Release kinetics profile of the electrospun membranes: (black) Acid, (red) Acid-PMB, (blue) OS, and (green) OS-PMB. (a) Full release kinetics profile (b) Profile of the PMB released after the first hour (PMB release up to 1 h is subtracted).

samples are similar. The PMB released after this burst comes from the molecule diffusion inside the PCL matrix towards the external medium. The higher crystallinity of the Acid membranes compared to the OS ones can explain the slower diffusion of the PMB inside the PCL matrix.

These results were in line with previous studies studying the release of PMB from electrospun polymers, where a burst was found in the first hours (up to 24 h) followed by a slower release [63–65] over 2–30 days. Yet, in those studies, the PMB was not directly encapsulated in the polymer but a carrier (i.e. modified silica, halloysite nanotubes) was used to encapsulate the PMB, which has a large influence on the encapsulation and release. Our results therefore show that similar results can be obtained with a simpler technique.

3.5. Antimicrobial evaluation

An agar diffusion test was performed using *S. aureus* (Gram +) and *P. aeruginosa* (Gram -) to assess the antimicrobial efficiency of the electrospun membranes. This test consisted of placing the membrane in direct contact with an agar plate seeded with bacteria. If the membrane presented an antimicrobial activity, the bacteria would have not grown around it and the agar would have remained transparent, forming an inhibition zone between the membrane and the beginning of the blurry zone. If the membrane did not present an antimicrobial activity, the bacteria would have grown around/on it and the agar would have become blurred. The size of the inhibition zones is presented in Table 5 while the pictures of the antimicrobial tests are shown in 4 of the supplementary information.

As expected, the controls (= Acid and OS) which do not contain PMB, did not present an antimicrobial activity (no inhibition zone and no growth under the sample). Regarding *S. aureus*, an antimicrobial activity was observed for the OS-PMB membrane with an inhibition zone of around 1.5 mm with no growth under the sample, while, for the Acid-PMB membrane, no inhibition zone was observed, only an inhibition of growth under the sample. Regarding *P. aeruginosa*, a clear antimicrobial activity was observed for the OS-PMB membranes (inhibition zone of about 5 mm and no growth under the sample) and the Acid-PMB (inhibition zone of about 0.6 mm and no growth under the sample). No significant difference could be observed between 24 and 48 h, meaning that the diffusion of PMB had already taken place after 24 h.

The difference between the OS-PMB and Acid-PMB is explained by different factors. First, the quantity released in 24 h by the OS-PMB is significantly higher than the one released by Acid-PMB, as shown in the previous section. Then, the activity of the PMB may have decreased due to its exposition to the acids.

The difference between *S. aureus* and *P. aeruginosa* comes from the activity of PMB against different bacterial strains. Indeed, PMB presents different minimum inhibitory concentration against these two strains (5 µg/mL for *P. aeruginosa* and 40 µg/mL for *S. aureus*, see 5 in the supplementary information). These results confirmed the results present in the literature. Indeed, it has been reported that PMB is usually used against Gram - bacteria [26,27] and is considered to be ineffective in the treatment of Gram + bacteria.

Table 5
Zone of inhibition (in mm, mean ± standard deviation) after 24 and 48 h of culture. / = no zone of inhibition and bacteria growth under the sample. 0 = no zone of inhibition and no bacteria growth under the sample.

	24 h		48 h	
Sample	**S. aureus**	**P. aeruginosa**	**S. aureus**	**P. aeruginosa**
Acid	/	/	/	/
Acid-PMB	0	0.6 ± 0.8	0	0.6 ± 0.8
OS	/	/	/	/
OS-PMB	1.5 ± 0.2	5.0 ± 0.2	1.4 ± 0.3	4.5 ± 0.3

3.6. Cytotoxicity

The cytotoxicity was checked via a XTT test following the ISO 10993–5 norm. The results can be seen in Fig. 7. A significant decrease in survival rate can be observed between the HDPE control and the samples. Yet, according to the ISO 10993 norm concerning the biological evaluation of medical devices, all samples can be considered as non-cytotoxic as they show a survival rate higher than 70 %. This also indicates that the membranes do not release any cytotoxic compounds. Statistical analysis indicated no significant differences among the samples. The innocuity of PCL and PMB was expected from previous studies [47,65].

3.7. Practical implications, limitations, and clinical perspectives

The electrospun PCL/PMB membranes developed in this study offer a number of practical advantages for wound care applications. The use of only two FDA-approved components—polycaprolactone and polymyxin B—simplifies the formulation and enhances the biocompatibility and regulatory acceptance of the system. Furthermore, the absence of complex carriers, surface treatments, or crosslinking agents makes the process highly reproducible and amenable to scale-up using existing industrial electrospinning platforms.

From a clinical perspective, the membranes exhibit sustained

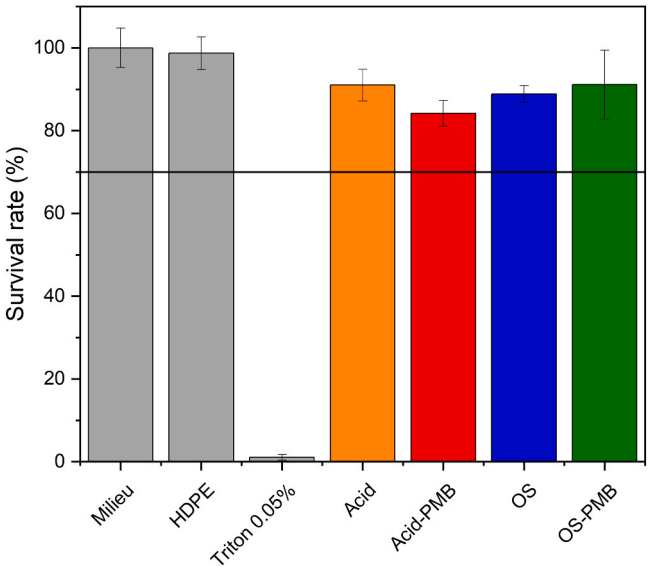

Fig. 7. Cytotoxicity results.

antimicrobial activity and favorable mechanical properties, suggesting their potential for use as dressings for infected or at-risk wounds. The duration of action is also advantageous, as these membranes remain effective for a longer period and therefore require less frequent changes than commercial products, which typically need to be replaced daily. The ability to modulate the release profile via the choice of solvent system could enable tailored treatments for different wound types or healing stages.

However, the present study also presents several limitations. First, the evaluation was limited to *in vitro* assays; *in vivo* testing is necessary to validate biocompatibility, healing efficacy, and real-time degradation behavior. Second, while solvent systems influenced drug release and membrane properties, long-term storage stability and sterilization compatibility remain to be assessed. Finally, the antibacterial performance was tested against two strains only; broader-spectrum studies, including biofilm models, would further strengthen the conclusions.

Despite these limitations, this work provides a promising foundation for developing practical, scalable, and safe antimicrobial wound dressings.

3.8. Comparisons

To contextualize our findings within the broader field of electrospun antimicrobial wound dressings, we compared our PCL/PMB membranes with similar systems from recent literature [66–69]. Table 6 summarizes key parameters, including materials, fiber morphology, mechanical properties, drug release kinetics, antimicrobial activity, and cytocompatibility. Our system, utilizing a simple two-component formulation with FDA-approved PCL and PMB, demonstrates comparable fiber diameters, tunable mechanical properties suitable for flexible wound sites, sustained release over 7 days with an initial burst for rapid action, strong antimicrobial efficacy against S. aureus and P. aeruginosa, and non-cytotoxic behavior (> 70 % cell survival). Notably, the choice of solvent systems (acidic vs. organic) allows modulation of release and antimicrobial performance, offering advantages in scalability and clinical translation over more complex multi-layer or hybrid designs.

Compared to recent literatures summarized in Table 6, the present PCL/PMB system is distinguished by its deliberate minimalism, being composed exclusively of two FDA-approved components, polycaprolactone and polymyxin B, without requiring additional polymers, natural polysaccharides, hydrogels, anticancer agents, multilayer architectures, nanoparticles, or chemical crosslinking. Despite this extreme simplicity, our single-layer membranes exhibit fiber diameters in the nanofibrous range comparable to or smaller than those reported in the referenced works, mechanical properties particularly well-suited to wounds located on mobile body areas thanks to their high elongation and conformability, and a sustained release of polymyxin B over seven days preceded by a marked and solvent-tunable initial burst that ensures rapid onset of antimicrobial action. The antibacterial efficacy against both Staphylococcus aureus and Pseudomonas aeruginosa, two of the

Table 6
Comparison with recent literature.

Study	Materials (Polymers/Drug)	Fiber Diameter (nm or µm)	Mechanical Properties	Drug Release Profile	Antimicrobial Activity	Cytocompatibility
This work	PCL/PMB (2 % w/w)	Nanofibrous (well-defined, tunable; specific values not quantified in morphology data)	Tunable; elongation and tensile suitable for mobile wounds (e.g., Acid: higher crystallinity, OS: lower)	Burst in first hour (higher for OS), then sustained up to 7 days (similar profiles post-burst)	Strong against S. aureus (OS: 1.5 mm inhibition zone, Acid: inhibition under sample) and P. aeruginosa (OS: 5 mm, Acid: 0.6 mm); no growth under samples	Non-cytotoxic (>70 % survival rate per ISO 10993–5; no significant differences among samples)
Viscusi et al. (2023) [69]	PCL-PVP/Quercetin (15 % wt)	PCL/PVP: 1.58 µm; Loaded: 2.34 µm	Not reported	Sustained over 7 days; plateau at 82 % (PBS) and 71 % (pH=3) after ~50 h; initial burst 78 % (PBS) and 63 % (pH=3) at 7 h	Not tested	Reduces viability: ~20 % (KG1 cells, direct contact, 72 h); ~40–80 % (MRC5 cells, conditioned medium, 24–48 h)
Song et al. (2024) [68]	Bilayer: Outer PCL/ENR (0.05–0.25 % w/v); Inner PCL-Gel/BLM (0.1 % w/v)	Nanofibers (specific diameters not reported)	Elongation at break: 26.35 ± 1.61 %; Tensile modulus: 15.25 ± 1.56 MPa	Not detailed (focus on loading and activity)	Excellent (bacteria not specified; outstanding against infections)	Good biocompatibility; promotes wound healing and inhibits A431 cell proliferation
Erdogan et al. (2025) [67]	Multi-layer: Outer/Inner PCL; Middle PCL-CS/Tig (3 % w/w)	PCL: 689 ± 186 nm; PCL-CS-Tig (single): 125 ± 19 nm; Multi-layer: 298 ± 98 nm	Tensile strength: 7.44 MPa	Biphasic; ~38 % in 60 min; follows Korsmeyer-Peppas kinetics (diffusion + relaxation)	Significant against E. coli and S. aureus (inhibition zones not quantified)	> 95 % viability (HUVECs, 2 days)
Nazemoroaia et al. (2025) [66]	Asymmetric: Bottom CS-Alg hydrogel/10-HDA (1–3 % w/v); Top PCL-SS	Electrospun top layer (specific diameters not reported)	Not reported (focus on swelling/degradation)	Not detailed (focus on loading and in vivo healing)	Demonstrated antibacterial properties	Enhanced cell proliferation at 1 % 10-HDA; accelerates in vivo wound healing without inflammation

most clinically problematic pathogens in chronic and burn wounds, remains strong and relevant, whereas several of the compared systems rely on natural compounds (quercetin, 10-HDA) with weaker or predominantly Gram-positive activity or require the addition of a second broad-spectrum antibiotic (enrofloxacin, tigecycline). Cytocompatibility is excellent and fully compliant with ISO 10993–5 (> 70 % cell viability), equivalent or superior to the best values reported in the literature and without the deliberate cytotoxicity toward cancer cell lines intentionally sought in certain oncological applications. Although sophisticated multilayer [67,68] or asymmetric hydrogel-nanofiber [66] designs offer complementary functionalities such as enhanced exudate absorption or immunomodulation, they significantly increase formulation complexity, production steps, cost, and regulatory burden. In contrast, the present single-step electrospun PCL/PMB platform, using only materials already approved by regulatory agencies, achieves comparable or superior performance across most critical parameters while remaining the simplest, most reproducible, and most readily scalable system among the recent comparable studies, thereby facilitating its industrial transfer and clinical translation.

4. Conclusions

In conclusion, the aim of the present project is the development of an electrospun membrane with antimicrobial properties for wound dressing applications. The membranes were developed by electrospinning PMB and PCL together. The impact of the selection of the solvents used for the electrospinning process (acids or organic solvents) on the physico-chemical properties of the membranes was studied. The results showed that the exposition of PCL with the acids lead to a degradation of the polymer but with low impact on the calorimetric properties of the membranes. The solvents nevertheless greatly affected the morphology and fiber size of the membranes, which in turns influenced the mechanical properties and conformability. Regarding the mechanical properties and conformability, the produced membranes proved to be in a suitable range to be used as wound dressing where a movement can be expected. The release of PMB was also assessed over 7 days. Both membranes presented a fast release over the first 1 h, with a larger release in the case of the membranes produced in the OS conditions. These membranes also showed the best antimicrobial results. Finally, all membranes were shown to be non-cytotoxic.

CRediT authorship contribution statement

Julien G. Mahy: formal analysis, investigation, writing – original draft, writing – review & editing. Stéphanie D. Lambert: methodology, formal analysis, writing – review & editing. Axel Lambert: investigation, formal analysis, writing – review & editing. Julie Bernard: investigation, formal analysis, writing – review & editing. Guérin Duysens: investigation, formal analysis, writing – review & editing. Ana Monteiro: investigation, formal analysis, writing – review & editing. Stéphane Dutrieux: investigation, formal analysis, writing – review & editing. Antoine Farcy: investigation, formal analysis, writing – review & editing. Raphaël Riva: investigation, formal analysis, writing – review & editing. Christine Jérôme: writing – review & editing. Olivier Jolois: writing – review & editing, supervision. Rémi G. Tikin: conceptualization, methodology, formal analysis, investigation, writing – original draft, writing – review & editing, supervision, funding acquisition, project administration.

Ethical approval

The authors declare that they have no known competing financial interests or personal relationships that could have appeared to influence the work reported in this paper.

Consent to participate

All authors agreed to participate in this work.

Consent to publish

All authors agreed to this version for publication.

Declaration of Competing Interest

The authors declare that they have no known competing financial interests or personal relationships that could have appeared to influence the work reported in this paper.

Acknowledgement

This work was supported by the Walloon Region via the project Demenciel (call: Win2Wal), SmartMultiDress (call: Win4Collective), and MicroEcoTex (call: Win4Collective).

The authors would like to thank Ludivine Fassotte and Maxime Houbben for their help and Camille Tilkin for the grammatical proofreading.

Julien G. Mahy and Stéphanie D. Lambert thank the F.R.S.-FNRS for his Postdoctoral Researcher, and her Research Director positions, respectively.

Appendix A. Supporting information

Supplementary data associated with this article can be found in the online version at doi:10.1016/j.nxmate.2025.101546.

Data availability

The raw/processed data required to reproduce these findings can be shared on demand.

References

[1] V. Ambrogi, D. Pietrella, A. Donnadio, L. Latterini, A. Di Michele, I. Luffarelli, M. Ricci, Biocompatible alginate silica supported silver nanoparticles composite films for wound dressing with antibiofilm activity, Mater. Sci. Eng. C. 112 (2020), https://doi.org/10.1016/j.msec.2020.110863.
[2] K.I. DragetAlginates Handb. Hydrocoll2009.
[3] F. Mo, M. Zhang, X. Duan, C. Lin, D. Sun, T. You, Recent Advances in Nanozymes for Bacteria-Infected Wound Therapy, Int. J. Nanomed. 17 (2022) 5947–5990, https://doi.org/10.2147/IJN.S382796.
[4] Z. Hussain, H.E. Thu, M. Rawas-Qalaji, M. Naseem, S. Khan, M. Sohail, Recent developments and advanced strategies for promoting burn wound healing, J. Drug Deliv. Sci. Technol. 68 (2022), https://doi.org/10.1016/j.jddst.2022.103092.
[5] C. Fan, Q. Xu, R. Hao, C. Wang, Y. Que, Y. Chen, C. Yang, J. Chang, Multifunctional wound dressings based on silicate bioactive materials, Biomaterials 287 (2022), https://doi.org/10.1016/j.biomaterials.2022.121652.
[6] A. Noor, A. Afzal, R. Masood, Z. Khaliq, S. Ahmad, F. Ahmad, M.B. Qadir, M. Irfan, Dressings for burn wound: a review, J. Mater. Sci. 57 (2022) 6536–6572, https://doi.org/10.1007/s10853-022-07056-4.
[7] S. Alven, S. Peter, Z. Mbese, B.A. Aderibigbe, Polymer-Based Wound Dressing Materials Loaded with Bioactive Agents: Potential Materials for the Treatment of Diabetic Wounds, Polymers 14 (2022), https://doi.org/10.3390/polym14040724.
[8] X. Liu, H. Xu, M. Zhang, D.G. Yu, Electrospun medicated nanofibers for wound healing: Review, Membranes 11 (2021), https://doi.org/10.3390/membranes11100770.
[9] K. Varaprasad, T. Jayaramudu, V. Kanikireddy, C. Toro, E.R. Sadiku, Alginate-based composite materials for wound dressing application:a mini review, Carbohydr. Polym. 236 (2020), https://doi.org/10.1016/j.carbpol.2020.116025.
[10] W. Shu, Y. Wang, X. Zhang, C. Li, H. Le, F. Chang, Functional hydrogel dressings for treatment of burn wounds, Front Bioeng. Biotechnol. 9 (2021), https://doi.org/10.3389/fbioe.2021.788461.
[11] B.A. Aderibigbe, B. Buyana, Alginate in wound dressings, Pharmaceutics 10 (2018), https://doi.org/10.3390/pharmaceutics10020042.
[12] M.S. Islam, B.C. Ang, A. Andriyana, A.M. Afifi, A review on fabrication of nanofibers via electrospinning and their applications, SN Appl. Sci. 1 (2019), https://doi.org/10.1007/s42452-019-1288-4.
[13] Y. Sun, S. Cheng, W. Lu, Y. Wang, P. Zhang, Q. Yao, Electrospun fibers and their application in drug controlled release, biological dressings, tissue repair, and

enzyme immobilization, RSC Adv. 9 (2019) 25712–25729, https://doi.org/10.1039/c9ra05012d.
[14] J. Xue, T. Wu, Y. Dai, Y. Xia, Electrospinning and electrospun nanofibers: methods, materials, and applications, Chem. Rev. 119 (2019) 5298–5415, https://doi.org/10.1021/acs.chemrev.8b00593.
[15] P. Wang, H. Lv, X. Cao, Y. Liu, D.G. Yu, Recent Progress of the Preparation and Application of Electrospun Porous Nanofibers, Polymers 15 (2023), https://doi.org/10.3390/polym15040921.
[16] X. Ou, W. Guo, H. Tian, D. Yu, R. Li, G. Gao, W. Qu, Portable direct spraying porous nanofibrous membranes stent-loaded polymyxin B for treating diabetic wounds with difficult-to-heal gram-negative bacterial infections, Mater. Today Bio 29 (2024), https://doi.org/10.1016/j.mtbio.2024.101365.
[17] P.D. Yadav, P.V. Londhe, S.S. Chavan, D.D. Mohite, G.B. Firame, S.S. Kadam, M. J. Patil, M.I. Ansari, Electrospun composite nanofibers for wound healing: synthesis, characterization, and clinical potential of biopolymer-based materials, Discov. Mater. 4 (2024), https://doi.org/10.1007/s43939-024-00173-8.
[18] Q. Zheng, Y. Xi, Y. Weng, Functional electrospun nanofibers: fabrication, properties, and applications in wound-healing process, RSC Adv. 14 (2024) 3359–3378, https://doi.org/10.1039/d3ra07075a.
[19] Q. Qi, R. Li, C. Wang, G. Hou, C. Li, Embryonic perfect repair inspired electrospun nanofibers dressing with temperature-sensitive and antibacterial properties for wound healing, Front Microbiol. 14 (2023), https://doi.org/10.3389/fmicb.2023.1233559.
[20] X. Liu, L. Gao, S. Fu, W. Zhao, F. Wang, J. Gao, C. Li, H. Wu, L. Wang, Polycaprolactone nanofiber-alginate hydrogel interpenetrated skin substitute for regulation of wound-substitute interface, Mater. Des. 227 (2023), https://doi.org/10.1016/j.matdes.2023.111706.
[21] J. Pan, Q. Meng, L. Zhang, C. Zhang, S. Wu, H. Zhai, Electrospun amine-modified polysuccinimide/polycaprolactone nanofiber hydrogel dressings as antibacterial and hemostatic wound dressing applications, Colloids Surf. B Biointerfaces 252 (2025), https://doi.org/10.1016/j.colsurfb.2025.114648.
[22] Y. Li, H. Xu, W. Zhao, L. Zhang, S. Wu, Electrospun robust, biodegradable, bioactive, and nanostructured sutures to accelerate the chronic wound healing, Biofabrication 17 (2025), https://doi.org/10.1088/1758-5090/adacaf.
[23] M. Rahman, M. Kabir, T. Islam, Y. Wang, Q. Meng, H. Liu, S. Chen, S. Wu, Curcumin-loaded ZIF-8 nanomaterials: exploring drug loading efficiency and biomedical performance, ACS Omega (2025), https://doi.org/10.1021/acsomega.4c09945.
[24] M.O. Christen, F. Vercesi, Polycaprolactone: how a well-known and futuristic polymer has become an innovative collagen-stimulator in esthetics, Clin. Cosmet. Invest. Dermatol. 13 (2020) 31–48, https://doi.org/10.2147/CCID.S229054.
[25] A. Azari, A. Golchin, M.M. Maymand, F. Mansouri, A. Ardeshirylajimi, Electrospun polycaprolactone nanofibers: current research and applications in biomedical application, Adv. Pharm. Bull. 12 (2022) 658–672, https://doi.org/10.34172/apb.2022.070.
[26] M. Afzal, A.K. Vijay, F. Stapleton, M.D.P. Willcox, Susceptibility of ocular Staphylococcus aureus to antibiotics and multipurpose disinfecting solutions, Antibiotics 10 (2021), https://doi.org/10.3390/antibiotics10101203.
[27] A.P. Zavascki, L.Z. Goldani, J. Li, R.L. Nation, Polymyxin B for the treatment of multidrug-resistant pathogens: a critical review, J. Antimicrob. Chemother. 60 (2007) 1206–1215, https://doi.org/10.1093/jac/dkm357.
[28] T. Dai, Y.-Y. Huang, S.K. Sharma, J.T. Hashmi, D.B. Kurup, M.R. Hamblin, Topical antimicrobials for burn wound infections, Recent Pat. Antiinfect Drug Discov. 5 (2010) 124–151.
[29] B. Pant, M. Park, S.J. Park, Drug delivery applications of core-sheath nanofibers prepared by coaxial electrospinning: a review, Pharmaceutics 11 (2019), https://doi.org/10.3390/pharmaceutics11070305.
[30] B. Ekram, B.M. Abdel-Hady, A.M. El-Kady, S.M. Amr, A.I. Waley, O.W. Guirguis, Optimum parameters for the production of nano-scale electrospun polycaprolactone to be used as a biomedical material, Adv. Nat. Sci. Nanosci. Nanotechnol. 8 (2017), https://doi.org/10.1088/2043-6254/aa92b4.
[31] M. Rajeev, C.C. Helms, A study of the relationship between polymer solution entanglement and electrospun PCL fiber mechanics, Polymers 15 (2023), https://doi.org/10.3390/polym15234555.
[32] J.M. Anaya-Mancipe, A.C. de Figueiredo, L.G. Rabello, M.L. Dias, R.M. da Silva Moreira Thiré, Evaluation of the polycaprolactone hydrolytic degradation in acid solvent and its influence on the electrospinning process, J. Appl. Polym. Sci. 141 (2024), https://doi.org/10.1002/app.55662.
[33] A. Chinnakorn, Y. Soi-Ngoen, O. Weeranantanapan, P. Pakawanit, S. Maensiri, K. Srisom, P. Janphuang, N. Radacsi, W. Nuansing, Fabrication of 3D polycaprolactone macrostructures by 3D electrospinning, ACS Biomater. Sci. Eng. 10 (2024) 5336–5351, https://doi.org/10.1021/acsbiomaterials.4c00302.
[34] L. Du, H. Xu, Y. Zhang, F. Zou, Electrospinning of polycaprolatone nanofibers with DMF additive: the effect of solution proprieties on jet perturbation and fiber morphologies, Fibers Polym. 17 (2016) 751–759, https://doi.org/10.1007/s12221-016-6045-3.
[35] N. Kulpreechanan, T. Bunaprasert, R. RangkupanElectrospinning of polycaprolactone in dichloromethane/dimethylformamide solvent system Adv. Mat. Res.2014, 33734210.4028/www.scientific.net/AMR.849.337.
[36] A. Fernández-Tena, R.A. Pérez-Camargo, O. Coulembier, L. Sangroniz, N. Aranburu, G. Guerrica-Echevarria, G. Liu, D. Wang, D. Cavallo, A.J. Müller, Effect of Molecular Weight on the Crystallization and Melt Memory of Poly (ε-caprolactone) (PCL), Macromolecules 56 (2023) 4602–4620, https://doi.org/10.1021/acs.macromol.3c00234.
[37] O.H. Lowry, N.J. Rosebrough, A.L. Farr, R.J. Randall, Protein measurement with the folin phenol reagent, J. Biol. Chem. 193 (1951) 265–275.
[38] M. Bartnikowski, T.R. Dargaville, S. Ivanovski, D.W. Hutmacher, Degradation mechanisms of polycaprolactone in the context of chemistry, geometry and environment, Prog. Polym. Sci. 96 (2019) 1–20, https://doi.org/10.1016/j.progpolymsci.2019.05.004.
[39] G.P. Sailema-Palate, A. Vidaurre, A.F. Campillo, I. Castilla-Cortázar, A comparative study on Poly(ε-caprolactone) film degradation at extreme pH values, Polym. Degrad. Stab. 130 (2016) 118–125, https://doi.org/10.1016/j.polymdegradstab.2016.06.005.
[40] O. Ero-Phillips, M. Jenkins, A. Stamboulis, Tailoring CRystallinity of Electrospun Plla Fibres by Control of Electrospinning Parameters, Polymers 4 (2012) 1331–1348, https://doi.org/10.3390/polym4031331.
[41] X. Wang, H. Zhao, L.S. Turng, Q. Li, Crystalline morphology of electrospun poly (ε-caprolactone) (PCL) nanofibers, Ind. Eng. Chem. Res 52 (2013) 4939–4949, https://doi.org/10.1021/ie302185e.
[42] E.K. Kostakova, L. Meszaros, G. Maskova, L. Blazkova, T. Turcsan, D. Lukas, Crystallinity of electrospun and centrifugal spun polycaprolactone fibers: a comparative study, J. Nanomater 2017 (2017), https://doi.org/10.1155/2017/8952390.
[43] W.A. Herrera-Kao, M.I. Loría-Bastarrachea, Y. Pérez-Padilla, J.V. Cauich-Rodríguez, H. Vázquez-Torres, J.M. Cervantes-Uc, Thermal degradation of poly (caprolactone), poly(lactic acid), and poly(hydroxybutyrate) studied by TGA/FTIR and other analytical techniques, Polym. Bull. 75 (2018) 4191–4205, https://doi.org/10.1007/s00289-017-2260-3.
[44] C. Vogel, H.W. Siesler, Thermal degradation of poly(ε-caprolactone), poly(L-lactic acid) and their blends with poly(3-hydroxy-butyrate) studied by TGA/FT-IR spectroscopy, in, Macromol. Symp. (2008) 183–194, https://doi.org/10.1002/masy.200850520.
[45] O. Persenaire, M. Alexandre, P. Degée, P. Dubois, Mechanisms and kinetics of thermal degradation of poly(ε-caprolactone), Biomacromolecules 2 (2001) 288–294, https://doi.org/10.1021/bm0056310.
[46] L.A. Can-Herrera, A.I. Oliva, M.A.A. Dzul-Cervantes, O.F. Pacheco-Salazar, J. M. Cervantes-Uc, Morphological and mechanical properties of electrospun polycaprolactone scaffolds: effect of applied voltage, Polymers 13 (2021) 1–16, https://doi.org/10.3390/polym13040662.
[47] Â. Semitela, A.F. Girão, C. Fernandes, G. Ramalho, I. Bdikin, A. Completo, P.A.A. P. Marques, Electrospinning of bioactive polycaprolactone-gelatin nanofibres with increased pore size for cartilage tissue engineering applications, J. Biomater. Appl. 35 (2020) 471–484, https://doi.org/10.1177/0885328220940194.
[48] J.L. Ferreira, S. Gomes, C. Henriques, J.P. Borges, J.C. Silva, Electrospinning polycaprolactone dissolved in glacial acetic acid: Fiber production, nonwoven characterization, and in Vitro evaluation, J. Appl. Polym. Sci. 131 (2014), https://doi.org/10.1002/app.41068.
[49] S. Bongiovanni Abel, L. Liverani, A.R. Boccaccini, G.A. Abraham, Effect of benign solvents composition on poly(ε-caprolactone) electrospun fiber properties, Mater. Lett. 245 (2019) 86–89, https://doi.org/10.1016/j.matlet.2019.02.107.
[50] K.A.G. Katsogiannis, G.T. Vladisavljević, S. Georgiadou, Porous electrospun polycaprolactone (PCL) fibres by phase separation, Eur. Polym. J. 69 (2015) 284–295, https://doi.org/10.1016/j.eurpolymj.2015.01.028.
[51] L. Van Der Schueren, B. De Schoenmaker, Ö.I. Kalaoglu, K. De Clerck, An alternative solvent system for the steady state electrospinning of polycaprolactone, Eur. Polym. J. 47 (2011) 1256–1263, https://doi.org/10.1016/j.eurpolymj.2011.02.025.
[52] A. Repanas, W.F. Wolkers, Coaxial electrospinning as a process to engineer biodegradable polymeric scaffolds as drug delivery systems for anti-inflammatory and anti- thrombotic pharmaceutical agents, Clin. Exp. Pharm. 05 (2015), https://doi.org/10.4172/2161-1459.1000192.
[53] N.D. Bikiaris, I. Koumentakou, G. Michailidou, M. Kostoglou, M. Vlachou, P. Barmpalexis, E. Karavas, G.Z. Papageorgiou, Investigation of Molecular weight, polymer concentration and process parameters factors on the sustained release of the anti-multiple-sclerosis agent teriflunomide from poly(ε-caprolactone) electrospun nanofibrous matrices, Pharmaceutics 14 (2022), https://doi.org/10.3390/pharmaceutics14081693.
[54] F. Zamani, M. Amani Tehran, A. Abbasi, Fabrication of PCL nanofibrous scaffold with tuned porosity for neural cell culture, Prog. Biomater. 10 (2021) 151–160, https://doi.org/10.1007/s40204-021-00159-2.
[55] F. Croisier, A.S. Duwez, C. Jérôme, A.F. Léonard, K.O. Van Der Werf, P.J. Dijkstra, M.L. Bennink, Mechanical testing of electrospun PCL fibers, Acta Biomater. 8 (2012) 218–224, https://doi.org/10.1016/j.actbio.2011.08.015.
[56] L. Berhan, A.M. Sastry, On modeling bonds in fused, porous networks: 3D simulations of fibrous-particulate joints, J. Compos Mater. 37 (2003) 715–740, https://doi.org/10.1177/002199803029725.
[57] T.-H. Nguyen, B.-T. Lee, Fabrication and characterization of cross-linked gelatin electro-spun nano-fibers, J. Biomed. Sci. Eng. 03 (2010) 1117–1124, https://doi.org/10.4236/jbise.2010.312145.
[58] T. Rabiee, H. Yeganeh, R. Gharibi, Antimicrobial wound dressings with high mechanical conformability prepared through thiol-yne click photopolymerization reaction, Biomed. Mater. (Bristol) 14 (2019), https://doi.org/10.1088/1748-605X/ab16b8.
[59] A. Ní Annaidh, K. Bruyère, M. Destrade, M.D. Gilchrist, M. Otténio, Characterization of the anisotropic mechanical properties of excised human skin, J. Mech. Behav. Biomed. Mater. 5 (2012) 139–148, https://doi.org/10.1016/j.jmbbm.2011.08.016.
[60] M. Minsart, S. Van Vlierberghe, P. Dubruel, A. Mignon, Commercial wound dressings for the treatment of exuding wounds: an in-depth physico-chemical comparative study, Burns Trauma 10 (2022), https://doi.org/10.1093/burnst/tkac024.

[61] Y. Yang, H. Hu, Application of superabsorbent spacer fabrics as exuding wound dressing, Polymers 10 (2018), https://doi.org/10.3390/polym10020210.
[62] M. Waring, Martyn Butcher, An investigation into the conformability of wound dressings, Wounds UK 7 (2011) 14–24.
[63] Y. Huang, Z. Yuan, D. Zhao, F. Wang, K. Zhang, Y. Li, Y. Wen, C. Wang, Polymyxin B immobilized nanofiber sponge for endotoxin adsorption, Eur. Polym. J. 110 (2019) 69–75, https://doi.org/10.1016/j.eurpolymj.2018.11.008.
[64] X. Zhang, R. Guo, J. Xu, Y. Lan, Y. Jiao, C. Zhou, Y. Zhao, Poly(l-lactide)/halloysite nanotube electrospun mats as dual-drug delivery systems and their therapeutic efficacy in infected full-thickness burns, J. Biomater. Appl. 30 (2015) 512–525, https://doi.org/10.1177/0885328215593837.
[65] Z. Gounani, S. Pourianejad, M.A. Asadollahi, R.L. Meyer, J.M. Rosenholm, A. Arpanaei, Polycaprolactone-gelatin nanofibers incorporated with dual antibiotic-loaded carboxyl-modified silica nanoparticles, J. Mater. Sci. 55 (2020) 17134–17150, https://doi.org/10.1007/s10853-020-05253-7.
[66] M. Nazemoroaia, F. Bagheri, S.Z. Mirahmadi-Zare, F. Eslami-kaliji, A. Derakhshan, Asymmetric natural wound dressing based on porous chitosan-alginate hydrogel/electrospun PCL-silk sericin loaded by 10-HDA for skin wound healing: In vitro and in vivo studies, Int. J. Pharm. 668 (2025), https://doi.org/10.1016/j.ijpharm.2024.124976.
[67] S. Erdogan, S.N. Günes, Y.E. Bulbul, M. Eskitoros-Togay, N. Dilsiz, Design of multi-layer electrospun poly(ε-caprolactone)/chitosan nanofiber scaffolds loaded with tigecycline for controlled drug release and antibacterial wound healing, Int. J. Biol. Macromol. 322 (2025), https://doi.org/10.1016/j.ijbiomac.2025.146955.
[68] Y. Song, Q. Hu, S. Liu, G. Yao, H. Zhang, Electrospinning drug-loaded polycaprolactone/polycaprolactone-gelatin multi-functional bilayer nanofibers composite scaffold for postoperative wound healing of cutaneous squamous cell carcinoma, Biomed. Technol. 8 (2024) 65–80, https://doi.org/10.1016/j.bmt.2024.10.001.
[69] G. Viscusi, G. Paolella, E. Lamberti, I. Caputo, G. Gorrasi, Quercetin-loaded polycaprolactone-polyvinylpyrrolidone electrospun membranes for health application: design, characterization, modeling and cytotoxicity studies, Membranes 13 (2023), https://doi.org/10.3390/membranes13020242.